Search for Higgs boson production in dilepton and missing energy final states with 5.4 fb^{-1} of $p\bar{p}$ collisions at $\sqrt{s} = 1.96$ TeV

V.M. Abazov[37], B. Abbott[75], M. Abolins[64], B.S. Acharya[30], M. Adams[50], T. Adams[48], E. Aguilo[6], G.D. Alexeev[37], G. Alkhazov[41], A. Alton[64,a], G. Alverson[62], G.A. Alves[2], L.S. Ancu[36], M. Aoki[49], Y. Arnoud[14], M. Arov[59], A. Askew[48], B. Åsman[42], O. Atramentov[67], C. Avila[8], J. BackusMayes[82], F. Badaud[13], L. Bagby[49], B. Baldin[49], D.V. Bandurin[58], S. Banerjee[30], E. Barberis[62], A.-F. Barfuss[15], P. Baringer[57], J. Barreto[2], J.F. Bartlett[49], U. Bassler[18], D. Bauer[44], S. Beale[6], A. Bean[57], M. Begalli[3], M. Begel[73], C. Belanger-Champagne[42], L. Bellantoni[49], J.A. Benitez[64], S.B. Beri[28], G. Bernardi[17], R. Bernhard[23], I. Bertram[43], M. Besançon[18], R. Beuselinck[44], V.A. Bezzubov[40], P.C. Bhat[49], V. Bhatnagar[28], G. Blazey[51], S. Blessing[48], K. Bloom[66], A. Boehnlein[49], D. Boline[61], T.A. Bolton[58], E.E. Boos[39], G. Borissov[43], T. Bose[61], A. Brandt[78], R. Brock[64], G. Brooijmans[70], A. Bross[49], D. Brown[19], X.B. Bu[7], D. Buchholz[52], M. Buehler[81], V. Buescher[25], V. Bunichev[39], S. Burdin[43,b], T.H. Burnett[82], C.P. Buszello[44], P. Calfayan[26], B. Calpas[15], S. Calvet[16], E. Camacho-Pérez[34], J. Cammin[71], M.A. Carrasco-Lizarraga[34], E. Carrera[48], B.C.K. Casey[49], H. Castilla-Valdez[34], S. Chakrabarti[72], D. Chakraborty[51], K.M. Chan[55], A. Chandra[53], E. Cheu[46], S. Chevalier-Théry[18], D.K. Cho[61], S.W. Cho[32], S. Choi[33], B. Choudhary[29], T. Christoudias[44], S. Cihangir[49], D. Claes[66], J. Clutter[57], M. Cooke[49], W.E. Cooper[49], M. Corcoran[80], F. Couderc[18], M.-C. Cousinou[15], D. Cutts[77], M. Ćwiok[31], A. Das[46], G. Davies[44], K. De[78], S.J. de Jong[36], E. De La Cruz-Burelo[34], K. DeVaughan[66], F. Déliot[18], M. Demarteau[49], R. Demina[71], D. Denisov[49], S.P. Denisov[40], S. Desai[49], H.T. Diehl[49], M. Diesburg[49], A. Dominguez[66], T. Dorland[82], A. Dubey[29], L.V. Dudko[39], L. Duflot[16], D. Duggan[67], A. Duperrin[15], S. Dutt[28], A. Dyshkant[51], M. Eads[66], D. Edmunds[64], J. Ellison[47], V.D. Elvira[49], Y. Enari[17], S. Eno[60], H. Evans[53], A. Evdokimov[73], V.N. Evdokimov[40], G. Facini[62], A.V. Ferapontov[77], T. Ferbel[61,71], F. Fiedler[25], F. Filthaut[36], W. Fisher[64], H.E. Fisk[49], M. Fortner[51], H. Fox[43], S. Fuess[49], T. Gadfort[73], C.F. Galea[36], A. Garcia-Bellido[71], V. Gavrilov[38], P. Gay[13], W. Geist[19], W. Geng[15,64], D. Gerbaudo[68], C.E. Gerber[50], Y. Gershtein[67], D. Gillberg[6], G. Ginther[49,71], G. Golovanov[37], B. Gómez[8], A. Goussiou[82], P.D. Grannis[72], S. Greder[19], H. Greenlee[49], Z.D. Greenwood[59], E.M. Gregores[4], G. Grenier[20], Ph. Gris[13], J.-F. Grivaz[16], A. Grohsjean[18], S. Grünendahl[49], M.W. Grünewald[31], F. Guo[72], J. Guo[72], G. Gutierrez[49], P. Gutierrez[75], A. Haas[70,c], P. Haefner[26], S. Hagopian[48], J. Haley[62], I. Hall[64], L. Han[7], K. Harder[45], A. Harel[71], J.M. Hauptman[56], J. Hays[44], T. Hebbeker[21], D. Hedin[51], J.G. Hegeman[35], A.P. Heinson[47], U. Heintz[77], C. Hensel[24], I. Heredia-De La Cruz[34], K. Herner[63], G. Hesketh[62], M.D. Hildreth[55], R. Hirosky[81], T. Hoang[48], J.D. Hobbs[72], B. Hoeneisen[12], M. Hohlfeld[25], S. Hossain[75], P. Houben[35], Y. Hu[72], Z. Hubacek[10], N. Huske[17], V. Hynek[10], I. Iashvili[69], R. Illingworth[49], A.S. Ito[49], S. Jabeen[61], M. Jaffré[16], S. Jain[69], D. Jamin[15], R. Jesik[44], K. Johns[46], C. Johnson[70], M. Johnson[49], D. Johnston[66], A. Jonckheere[49], P. Jonsson[44], A. Juste[49,d], E. Kajfasz[15], D. Karmanov[39], P.A. Kasper[49], I. Katsanos[66], V. Kaushik[78], R. Kehoe[79], S. Kermiche[15], N. Khalatyan[49], A. Khanov[76], A. Kharchilava[69], Y.N. Kharzheev[37], D. Khatidze[77], M.H. Kirby[52], M. Kirsch[21], J.M. Kohli[28], A.V. Kozelov[40], J. Kraus[64], A. Kumar[69], A. Kupco[11], T. Kurča[20], V.A. Kuzmin[39], J. Kvita[9], D. Lam[55], S. Lammers[53], G. Landsberg[77], P. Lebrun[20], H.S. Lee[32], W.M. Lee[49], A. Leflat[39], J. Lellouch[17], L. Li[47], Q.Z. Li[49], S.M. Lietti[5], J.K. Lim[32], D. Lincoln[49], J. Linnemann[64], V.V. Lipaev[40], R. Lipton[49], Y. Liu[7], Z. Liu[6], A. Lobodenko[41], M. Lokajicek[11], P. Love[43], H.J. Lubatti[82], R. Luna-Garcia[34,e], A.L. Lyon[49], A.K.A. Maciel[2], D. Mackin[80], P. Mättig[27], R. Magaña-Villalba[34], P.K. Mal[46], S. Malik[66], V.L. Malyshev[37], Y. Maravin[58], J. Martínez-Ortega[34], R. McCarthy[72], C.L. McGivern[57], M.M. Meijer[36], A. Melnitchouk[65], L. Mendoza[8], D. Menezes[51], P.G. Mercadante[4], M. Merkin[39], A. Meyer[21], J. Meyer[24], N.K. Mondal[30], T. Moulik[57], G.S. Muanza[15], M. Mulhearn[81], O. Mundal[22], L. Mundim[3], E. Nagy[15], M. Naimuddin[29], M. Narain[77], R. Nayyar[29], H.A. Neal[63], J.P. Negret[8], P. Neustroev[41], H. Nilsen[23], H. Nogima[3], S.F. Novaes[5], T. Nunnemann[26], G. Obrant[41], D. Onoprienko[58], J. Orduna[34], N. Osman[44], J. Osta[55], R. Otec[10], G.J. Otero y Garzón[1], M. Owen[45], M. Padilla[47], P. Padley[80], M. Pangilinan[77], N. Parashar[54], V. Parihar[77], S.-J. Park[24], S.K. Park[32], J. Parsons[70], R. Partridge[77], N. Parua[53], A. Patwa[73], B. Penning[49], M. Perfilov[39], K. Peters[45], Y. Peters[45], P. Pétroff[16], R. Piegaia[1], J. Piper[64], M.-A. Pleier[73], P.L.M. Podesta-Lerma[34,f], V.M. Podstavkov[49], M.-E. Pol[2], P. Polozov[38], A.V. Popov[40], M. Prewitt[80], D. Price[53], S. Protopopescu[73], J. Qian[63], A. Quadt[24], B. Quinn[65], M.S. Rangel[16], K. Ranjan[29], P.N. Ratoff[43], I. Razumov[40], P. Renkel[79], P. Rich[45], M. Rijssenbeek[72], I. Ripp-Baudot[19], F. Rizatdinova[76], S. Robinson[44], M. Rominsky[75], C. Royon[18], P. Rubinov[49], R. Ruchti[55], G. Safronov[38], G. Sajot[14], A. Sánchez-Hernández[34], M.P. Sanders[26], B. Sanghi[49], G. Savage[49], L. Sawyer[59], T. Scanlon[44], D. Schaile[26],

arXiv:1001.4481v1 [hep-ex] 25 Jan 2010

R.D. Schamberger[72], Y. Scheglov[41], H. Schellman[52], T. Schliephake[27], S. Schlobohm[82], C. Schwanenberger[45], R. Schwienhorst[64], J. Sekaric[57], H. Severini[75], E. Shabalina[24], V. Shary[18], A.A. Shchukin[40], R.K. Shivpuri[29], V. Simak[10], V. Sirotenko[49], P. Skubic[75], P. Slattery[71], D. Smirnov[55], G.R. Snow[66], J. Snow[74], S. Snyder[73], S. Söldner-Rembold[45], L. Sonnenschein[21], A. Sopczak[43], M. Sosebee[78], K. Soustruznik[9], B. Spurlock[78], J. Stark[14], V. Stolin[38], D.A. Stoyanova[40], J. Strandberg[63], M.A. Strang[69], E. Strauss[72], M. Strauss[75], R. Ströhmer[26], D. Strom[50], L. Stutte[49], P. Svoisky[36], M. Takahashi[45], A. Tanasijczuk[1], W. Taylor[6], B. Tiller[26], M. Titov[18], V.V. Tokmenin[37], D. Tsybychev[72], B. Tuchming[18], C. Tully[68], P.M. Tuts[70], R. Unalan[64], L. Uvarov[41], S. Uvarov[41], S. Uzunyan[51], P.J. van den Berg[35], R. Van Kooten[53], W.M. van Leeuwen[35], N. Varelas[50], E.W. Varnes[46], I.A. Vasilyev[40], P. Verdier[20], L.S. Vertogradov[37], M. Verzocchi[49], M. Vesterinen[45], D. Vilanova[18], P. Vint[44], P. Vokac[10], H.D. Wahl[48], M.H.L.S. Wang[71], J. Warchol[55], G. Watts[82], M. Wayne[55], G. Weber[25], M. Weber[49,g], M. Wetstein[60], A. White[78], D. Wicke[25], M.R.J. Williams[43], G.W. Wilson[57], S.J. Wimpenny[47], M. Wobisch[59], D.R. Wood[62], T.R. Wyatt[45], Y. Xie[49], C. Xu[63], S. Yacoob[52], R. Yamada[49], W.-C. Yang[45], T. Yasuda[49], Y.A. Yatsunenko[37], Z. Ye[49], H. Yin[7], K. Yip[73], H.D. Yoo[77], S.W. Youn[49], J. Yu[78], C. Zeitnitz[27], S. Zelitch[81], T. Zhao[82], B. Zhou[63], J. Zhu[72], M. Zielinski[71], D. Zieminska[53], L. Zivkovic[70], V. Zutshi[51], and E.G. Zverev[39]

(The DØ Collaboration)

[1] *Universidad de Buenos Aires, Buenos Aires, Argentina*
[2] *LAFEX, Centro Brasileiro de Pesquisas Físicas, Rio de Janeiro, Brazil*
[3] *Universidade do Estado do Rio de Janeiro, Rio de Janeiro, Brazil*
[4] *Universidade Federal do ABC, Santo André, Brazil*
[5] *Instituto de Física Teórica, Universidade Estadual Paulista, São Paulo, Brazil*
[6] *Simon Fraser University, Burnaby, British Columbia, Canada; and York University, Toronto, Ontario, Canada*
[7] *University of Science and Technology of China, Hefei, People's Republic of China*
[8] *Universidad de los Andes, Bogotá, Colombia*
[9] *Center for Particle Physics, Charles University, Faculty of Mathematics and Physics, Prague, Czech Republic*
[10] *Czech Technical University in Prague, Prague, Czech Republic*
[11] *Center for Particle Physics, Institute of Physics, Academy of Sciences of the Czech Republic, Prague, Czech Republic*
[12] *Universidad San Francisco de Quito, Quito, Ecuador*
[13] *LPC, Université Blaise Pascal, CNRS/IN2P3, Clermont, France*
[14] *LPSC, Université Joseph Fourier Grenoble 1, CNRS/IN2P3, Institut National Polytechnique de Grenoble, Grenoble, France*
[15] *CPPM, Aix-Marseille Université, CNRS/IN2P3, Marseille, France*
[16] *LAL, Université Paris-Sud, IN2P3/CNRS, Orsay, France*
[17] *LPNHE, IN2P3/CNRS, Universités Paris VI and VII, Paris, France*
[18] *CEA, Irfu, SPP, Saclay, France*
[19] *IPHC, Université de Strasbourg, CNRS/IN2P3, Strasbourg, France*
[20] *IPNL, Université Lyon 1, CNRS/IN2P3, Villeurbanne, France and Université de Lyon, Lyon, France*
[21] *III. Physikalisches Institut A, RWTH Aachen University, Aachen, Germany*
[22] *Physikalisches Institut, Universität Bonn, Bonn, Germany*
[23] *Physikalisches Institut, Universität Freiburg, Freiburg, Germany*
[24] *II. Physikalisches Institut, Georg-August-Universität Göttingen, Göttingen, Germany*
[25] *Institut für Physik, Universität Mainz, Mainz, Germany*
[26] *Ludwig-Maximilians-Universität München, München, Germany*
[27] *Fachbereich Physik, University of Wuppertal, Wuppertal, Germany*
[28] *Panjab University, Chandigarh, India*
[29] *Delhi University, Delhi, India*
[30] *Tata Institute of Fundamental Research, Mumbai, India*
[31] *University College Dublin, Dublin, Ireland*
[32] *Korea Detector Laboratory, Korea University, Seoul, Korea*
[33] *SungKyunKwan University, Suwon, Korea*
[34] *CINVESTAV, Mexico City, Mexico*
[35] *FOM-Institute NIKHEF and University of Amsterdam/NIKHEF, Amsterdam, The Netherlands*
[36] *Radboud University Nijmegen/NIKHEF, Nijmegen, The Netherlands*
[37] *Joint Institute for Nuclear Research, Dubna, Russia*
[38] *Institute for Theoretical and Experimental Physics, Moscow, Russia*
[39] *Moscow State University, Moscow, Russia*
[40] *Institute for High Energy Physics, Protvino, Russia*

[41] *Petersburg Nuclear Physics Institute, St. Petersburg, Russia*
[42] *Stockholm University, Stockholm, Sweden, and Uppsala University, Uppsala, Sweden*
[43] *Lancaster University, Lancaster, United Kingdom*
[44] *Imperial College London, London SW7 2AZ, United Kingdom*
[45] *The University of Manchester, Manchester M13 9PL, United Kingdom*
[46] *University of Arizona, Tucson, Arizona 85721, USA*
[47] *University of California, Riverside, California 92521, USA*
[48] *Florida State University, Tallahassee, Florida 32306, USA*
[49] *Fermi National Accelerator Laboratory, Batavia, Illinois 60510, USA*
[50] *University of Illinois at Chicago, Chicago, Illinois 60607, USA*
[51] *Northern Illinois University, DeKalb, Illinois 60115, USA*
[52] *Northwestern University, Evanston, Illinois 60208, USA*
[53] *Indiana University, Bloomington, Indiana 47405, USA*
[54] *Purdue University Calumet, Hammond, Indiana 46323, USA*
[55] *University of Notre Dame, Notre Dame, Indiana 46556, USA*
[56] *Iowa State University, Ames, Iowa 50011, USA*
[57] *University of Kansas, Lawrence, Kansas 66045, USA*
[58] *Kansas State University, Manhattan, Kansas 66506, USA*
[59] *Louisiana Tech University, Ruston, Louisiana 71272, USA*
[60] *University of Maryland, College Park, Maryland 20742, USA*
[61] *Boston University, Boston, Massachusetts 02215, USA*
[62] *Northeastern University, Boston, Massachusetts 02115, USA*
[63] *University of Michigan, Ann Arbor, Michigan 48109, USA*
[64] *Michigan State University, East Lansing, Michigan 48824, USA*
[65] *University of Mississippi, University, Mississippi 38677, USA*
[66] *University of Nebraska, Lincoln, Nebraska 68588, USA*
[67] *Rutgers University, Piscataway, New Jersey 08855, USA*
[68] *Princeton University, Princeton, New Jersey 08544, USA*
[69] *State University of New York, Buffalo, New York 14260, USA*
[70] *Columbia University, New York, New York 10027, USA*
[71] *University of Rochester, Rochester, New York 14627, USA*
[72] *State University of New York, Stony Brook, New York 11794, USA*
[73] *Brookhaven National Laboratory, Upton, New York 11973, USA*
[74] *Langston University, Langston, Oklahoma 73050, USA*
[75] *University of Oklahoma, Norman, Oklahoma 73019, USA*
[76] *Oklahoma State University, Stillwater, Oklahoma 74078, USA*
[77] *Brown University, Providence, Rhode Island 02912, USA*
[78] *University of Texas, Arlington, Texas 76019, USA*
[79] *Southern Methodist University, Dallas, Texas 75275, USA*
[80] *Rice University, Houston, Texas 77005, USA*
[81] *University of Virginia, Charlottesville, Virginia 22901, USA and*
[82] *University of Washington, Seattle, Washington 98195, USA*

D0 Collaboration

(Dated: January 25, 2010)

A search for the standard model Higgs boson is presented using events with two charged leptons and large missing transverse energy selected from 5.4 fb^{-1} of integrated luminosity in $p\overline{p}$ collisions at $\sqrt{s} = 1.96$ TeV collected with the D0 detector at the Fermilab Tevatron Collider. No significant excess of events above background predictions is found, and observed (expected) upper limits at 95% confidence level on the rate of Higgs boson production are derived that are a factor of 1.55 (1.36) above the predicted standard model cross section at m_H=165 GeV.

PACS numbers: 13.85.Rm, 14.80.Bn

The Higgs mechanism, introduced in the standard model (SM) to explain electroweak symmetry breaking, predicts a massive scalar (Higgs) boson, which has yet to be observed. Direct searches at the CERN LEP e^+e^- collider yielded a lower limit of 114.4 GeV for the SM Higgs boson mass at 95% confidence level (C.L.) [8]. Indirect constraints obtained from fits to precision electroweak data, when combined with direct searches at LEP, give an upper bound of 186 GeV at 95% C.L. [9]. For a Higgs boson mass (m_H) close to 165 GeV the product of the SM Higgs boson production cross section and the decay branching ratio into two W bosons is maximal [10] and motivates the analysis strategy.

In this Letter we present a search for Higgs bosons in

final states containing two charged leptons and missing transverse energy ($\not\!\!E_T$) using data collected with the D0 detector [11] and corresponding to an integrated luminosity of 5.4 fb^{-1} of $p\bar{p}$ collisions at $\sqrt{s} = 1.96$ TeV. We consider final states containing either an electron and a positron (e^+e^-), an electron or a positron and a muon ($e^\pm\mu^\mp$), or two muons ($\mu^+\mu^-$). Final states with tau leptons decaying to e or μ or where hadronic tau decays are misidentified as electrons will also contribute to our search.

Previous searches in this channel have been performed at the Tevatron by the CDF and the D0 collaborations [12, 13]. This search represents an almost twenty-fold increase in the D0 data set and considers additional Higgs boson production modes leading to the dilepton and $\not\!\!E_T$ signature. In addition, the lepton acceptance is improved and the separation of background and signal processes now utilises an artificial neural network (NN) event classification technique. The main Higgs boson production modes are via gluon fusion and vector boson fusion. For these production modes, this analysis considers only the Higgs boson decay $H \to WW^{(*)} \to \ell\ell'\nu\nu'$ ($\ell, \ell' = e, \mu, \tau$). Also considered is Higgs boson production in association with a W or Z boson, where Higgs boson decays to W/Z bosons and leptons yield a dilepton plus $\not\!\!E_T$ signature. The overlap with events considered in the analysis of $WH \to Wb\bar{b}$ and $ZH \to Zb\bar{b}$ final states [15] is negligible. The CDF collaboration is also reporting an updated search in this channel [14].

The main background processes for this analysis are pair production of heavy gauge bosons, $W(+\text{jets}/\gamma)$ and $Z/\gamma^*(+\text{jets}/\gamma)$ production, $t\bar{t}$ production and multijet production in which jets are misidentified as leptons. To model the $W(+\text{jets}/\gamma)$ and $Z/\gamma^*(+\text{jets}/\gamma)$ backgrounds we use the ALPGEN event generator [16]. The signal and remaining SM background processes are simulated with PYTHIA [17] and all Monte Carlo (MC) samples are generated using CTEQ6L1 [18] parton distribution functions (PDFs). In all cases, event generation is followed by a detailed GEANT-based [19] simulation of the D0 detector.

The background MC samples for inclusive W and Z/γ^* production are normalized to NNLO cross section predictions [20] calculated using MRST 2004 NNLO PDFs [21]. The rate of $t\bar{t}$ production is normalized to a NNLO calculation [22] and diboson rates (WW, WZ, and ZZ) are normalized to NLO cross sections [23]. The signal cross sections are calculated at NNLO [24] (at NLO in the case of the vector boson fusion process). The branching fractions for the Higgs boson decay are determined using HDECAY [25].

The simulated Z boson transverse momentum (p_T) distribution is modified to match the spectrum measured in data [26]. In order to simulate the W boson p_T distribution, the measured Z boson p_T spectrum is multiplied by the ratio of W to Z boson p_T distributions at NLO [27]. To improve the modeling of WW background, the p_T of the diboson system is modified to match that obtained using the MC@NLO generator [28], and the distribution of the opening angle of the two leptons is modified to take into account the contribution from gluon-gluon initiated processes [29]. The distribution of the transverse momentum of the Higgs boson generated in the gluon fusion process is modified to match that obtained using SHERPA [30].

The background due to multijet production, in which jets are misidentified as leptons, is determined from data. For this purpose, a sample of like-charged dilepton events is used in the $\mu^+\mu^-$ channel, corrected for like-charge contributions from non-multijet processes. The e^+e^- and $e^\pm\mu^\mp$ channels use a sample of events with inverted lepton quality requirements, scaled to match the yield and kinematics determined in the like-charge data.

This search is based on a sample of dilepton event candidates collected using a mixture of single and dilepton triggers which achieve close to 100% signal efficiency. The identification of electron and muon candidates is based on the criteria described in the previous search [13]. In addition to the track isolation criterion, a constraint on the scalar sum of charged particles transverse momentum (p_T) in a cone of radius $\mathcal{R} = \sqrt{(\Delta\phi)^2 + (\Delta\eta)^2} = 0.5$ [31] around the muon track, an isolation requirement in the calorimeter is applied. This is a requirement on the transverse energy deposited in an annulus $0.1 < \mathcal{R} < 0.4$ around the muon track. In the $e^\pm\mu^\mp$ channel, each of these isolation parameters divided by the muon p_T is required to be < 0.15, whereas in the $\mu^+\mu^-$ channel the ratio of the sum of these two quantities divided by the muon p_T is required to be $< 0.4(0.5)$ for the highest (next-to-highest) p_T lepton ℓ_1 (ℓ_2). In the $\mu^+\mu^-$ channel, the product of the isolation ratios for both muons is required to be < 0.06.

Electrons are required to have $|\eta| < 2.5$ (< 2.0 in the e^+e^- channel), and muons $|\eta| < 2.0$. Both leptons are required to originate from the same interaction vertex and to have opposite charges. Electrons must have $p_T^e > 15$ GeV, and muons $p_T^\mu > 10$ GeV. In the $\mu^+\mu^-$ channel one of the two muons is required to have $p_T^\mu > 20$ GeV. In addition, the dilepton invariant mass is required to exceed 15 GeV. Jets are reconstructed in the calorimeter using an iterative midpoint cone algorithm [32] with a radius $\mathcal{R} = 0.5$ and are required to have $p_T^{\text{jet}} > 15$ GeV and $|\eta| < 2.4$. No jet-based event selection is applied, since the number of jets in the event is used in the NN to help discriminate signal from background. In the $\mu^+\mu^-$ channel, both muons must be separated from any jet by $\mathcal{R} > 0.1$. This stage of the analysis is referred to as "preselection".

After preselection, the background is dominated by Z/γ^* production. This background is suppressed by requiring $\not\!\!E_T > 20$ GeV (> 25 GeV in the $\mu^+\mu^-$ channel). Events are also removed if the $\not\!\!E_T$ was likely produced by a mismeasurement of jet energies by requiring for the

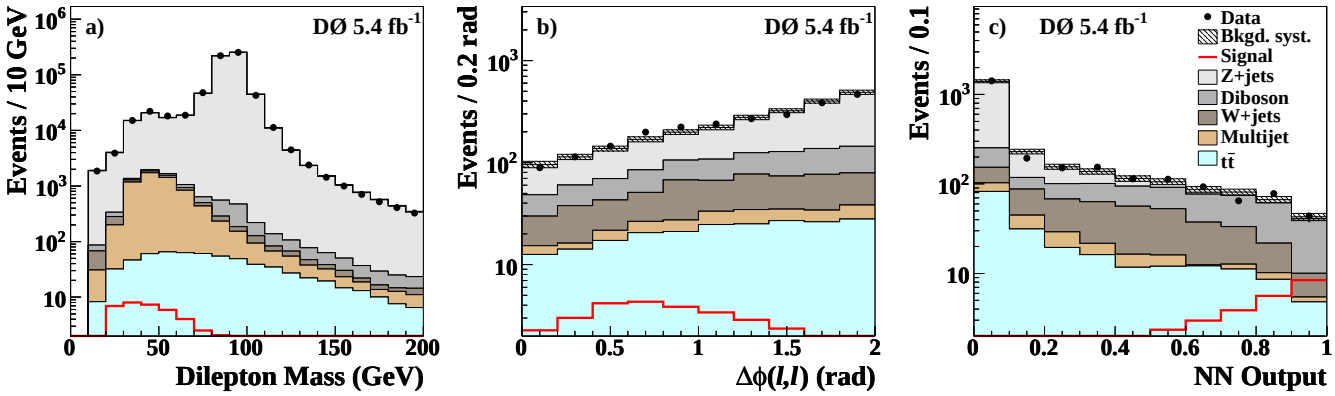

FIG. 1: (color online) (a) The dilepton invariant mass after preselection; (b) the $\Delta\phi(\ell,\ell)$ angle after final selection; and (c) the neural network output after final selection. The signal is shown for m_H=165 GeV. The systematic uncertainty is shown after fitting (see text for details).

scaled $\not\!\!E_T$ [13], $\not\!\!E_T^{\rm Sc} > 6$ in the e^+e^- and $e^\pm\mu^\mp$ channels. The minimum transverse mass, $M_T^{\rm min}$(defined as the smaller of the transverse masses M_T [33] calculated from the $\not\!\!E_T$ and either of the two leptons), is required to be > 20 GeV (> 30 GeV in the e^+e^- channel) to suppress backgrounds where $\not\!\!E_T$ originates from mismeasured lepton energy. Finally, events are rejected by requiring for the azimuthal opening angle between the two leptons $\Delta\phi(\ell,\ell) < 2.0$ rad, because leptons from background processes tend to be back-to-back in the transverse plane, in contrast with those from a Higgs boson decay which, owing to its zero spin, tend to move in the same direction. This stage of the analysis is referred to as "final selection".

The dilepton invariant mass distribution after preselection for the combination of the three channels is shown in Fig. 1(a). The $\Delta\phi(\ell,\ell)$ distribution after final selection is shown in Fig. 1(b). The contributions from the different background processes in each of the three channels are compared with the numbers of events observed in data after preselection and after final selection in Table I. The total systematic uncertainty (described below and in the supplemental material) after fitting is shown with correlations appropriately incorporated.

To improve the separation between signal and background, an optimized NN is used in each of the three channels. Several well-modeled discriminant variables are used as inputs to the NN: the transverse momenta of the leptons, a variable indicating the quality of the leptons' identification, the transverse momentum and invariant mass of the dilepton system, $M_T^{\rm min}$, $\not\!\!E_T$, $\not\!\!E_T^{\rm Sc}$, $\Delta\phi(\ell,\ell)$, $\Delta\phi(\ell_1,\not\!\!E_T)$, $\Delta\phi(\ell_2,\not\!\!E_T)$, the number of identified jets, and the scalar sum of the transverse momenta of the jets. In each channel, separate NNs are trained for 18 test values of m_H from 115 to 200 GeV in steps of 5 GeV. The combined distribution of the NN output for $m_H = 165$ GeV from all three channels is shown in Fig. 1(c).

The estimates for the expected number of background and signal events depend on numerous factors, each introducing a source of systematic uncertainty. Two types of systematic uncertainties have been considered: those affecting the absolute predicted event yield and those which also affect the shape of the NN output distribution. The most significant systematic uncertainties affecting the normalization of the NN output (quoted as a percentage of the yield per signal or background process) are: lepton reconstruction efficiencies (3–6%), lepton momentum calibration (1–3%), theoretical cross section (including PDF, factorization and renormalization scale uncertainties: 7% for diboson, 10% for $t\bar{t}$ 7% for W/Z(+jets), 11% for Higgs signal), modeling of multijet background (2–15)%, and integrated luminosity (6.1%). The most important sources affecting the NN output shape are: jet reconstruction efficiency (1–3%), jet energy scale calibration (1–5%), jet energy resolution (2%), and modeling of $p_T(WW)$, $p_T(H)$, and $p_T(Z)$ (1–5)%. The systematic uncertainty on the modeling of $p_T(WW)$ and $p_T(H)$ has been determined by comparing the p_T distributions of PYTHIA, SHERPA, and MC@NLO, and the uncertainty on $p_T(Z)$ from a comparison of the shape of the NN distribution between data and MC in a Z/γ^* enriched control sample. The SHERPA and MC@NLO predictions agree well with each other and generate harder p_T spectra than PYTHIA [34]. The uncertainty on $\Delta\phi(\ell,\ell)$ for the WW background is taken as 30% of the correction to the PYTHIA angular distribution as estimated in Ref. [29], leading to a relative uncertainty at the subpercent level. Appropriate correlations of systematic uncertainties between different channels, between different backgrounds, and between backgrounds and signal are included.

TABLE I: Expected and observed event yields in each channel after preselection and at the final selection. The systematic uncertainty after fitting is shown for all samples at final selection.

	$e^{\pm}\mu^{\mp}$		$e^{+}e^{-}$		$\mu^{+}\mu^{-}$	
	preselection	final selection	preselection	final selection	preselection	final selection
$Z/\gamma^{*} \to e^{+}e^{-}$	120	< 0.1	274886	158 ± 13	–	–
$Z/\gamma^{*} \to \mu^{+}\mu^{-}$	89	4.3 ± 0.3	–	–	373582	1247 ± 37
$Z/\gamma^{*} \to \tau^{+}\tau^{-}$	3871	7.1 ± 0.5	1441	0.7 ± 0.1	2659	12.0 ± 0.7
$t\bar{t}$	312	93.8 ± 8.3	159	47.0 ± 4.4	184	74.6 ± 6.8
W + jets/γ	267	112 ± 9	308	122 ± 11	236	91.5 ± 6.5
WW	455	165 ± 6	202	73.9 ± 6.4	272	107 ± 9
WZ	23.6	7.6 ± 0.2	137	11.5 ± 1.0	171	21.5 ± 2.0
ZZ	5.4	0.6 ± 0.1	117	9.3 ± 0.9	147	18.0 ± 1.8
Multijet	430	6.4 ± 2.5	1370	1.0 ± 0.1	408	53.8 ± 10.3
Signal ($m_H = 165$ GeV)	18.8	13.5 ± 1.5	11.2	7.2 ± 0.8	12.7	9.0 ± 1.0
Total background	5573	397 ± 14	278620	423 ± 19	377659	1625 ± 41
Data	5566	390	278277	421	384083	1613

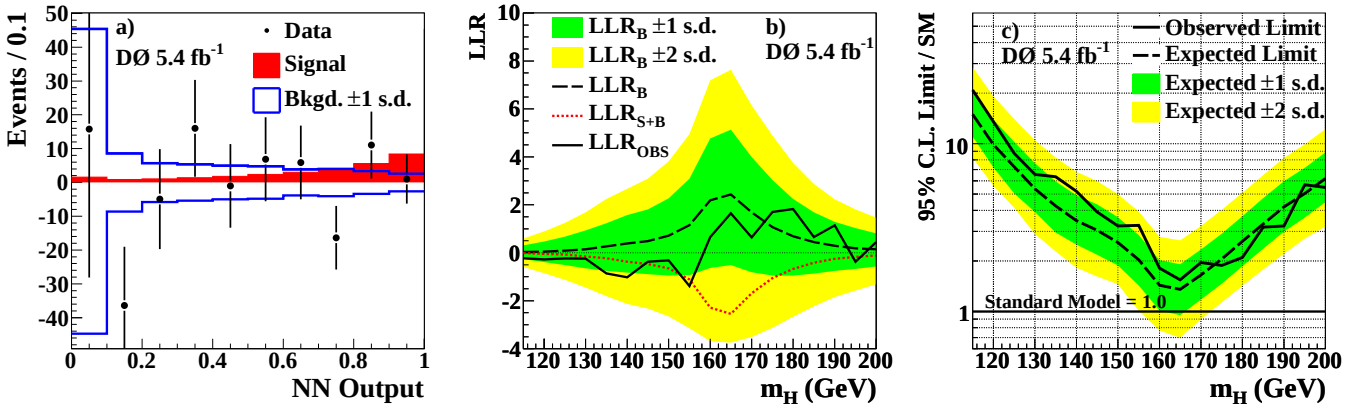

FIG. 2: (color online) (a) Data after subtracting the fitted background (points) and SM signal expectation (filled histogram) as a function of the NN output for m_H=165 GeV. Also shown is the ±1 standard deviation (s.d.) band on the total background after fitting. (b) Observed LLR (solid line), expected LLR for background-only hypothesis (dashed line), and signal + background hypothesis (dotted line). (c) Upper limit on Higgs boson production cross section at 95% C.L. expressed as a ratio to the SM cross section. The one and two s.d. bands around the curve corresponding to the background-only hypothesis are also shown.

After all selections, no significant excess of signal-like events is observed for any test value of m_H. Thus the NN output distributions are used to set upper limits on the Higgs boson production cross section, assuming the SM-predicted ratio of production cross sections and Higgs decay branching ratios. Upper limits are set using the three search channels combined using a modified frequentist method with a log-likelihood ratio (LLR) test statistic [35]. To minimize the degrading effects of systematics on the search sensitivity, the signal and different background sources contributions are fitted to the data observations by maximizing a likelihood function over the systematic uncertainties for both the background only and signal+background hypotheses [36]. Figure 2(a) shows a comparison of the NN distribution between background-subtracted data and the expected signal for m_H=165 GeV hypothesis. The background prediction and its uncertainties have been determined from the fit to data under the background-only hypothesis. The LLR distribution as a function of m_H is shown in Figure 2(b) demonstrating the overall consistency of the data with the background-only hypothesis in the full m_H range considered. Table II and Figure 2(c) present the expected and observed upper limits as a ratio to the expected SM cross section. Assuming m_H=165 GeV, the observed (expected) upper limit at 95% C.L. on Higgs boson production is a factor of 1.55 (1.36) times the SM cross section, representing an improvement in sensitivity of over a factor of six relative to our previous publication [13], larger than expected from the luminosity increase alone.

Auxiliary material is provided in [37].

We thank the staffs at Fermilab and collaborating institutions, and acknowledge support from the DOE

TABLE II: Expected and observed upper limits at 95% C.L. for Higgs boson production cross section expressed as a ratio to the cross section predicted by the SM for a range of test Higgs boson masses.

m_H (GeV)	115	120	125	130	135	140	145	150	155	160	165	170	175	180	185	190	195	200
Limit (exp.)	14.9	9.74	7.20	5.40	4.23	3.48	3.07	2.58	2.02	1.43	1.36	1.65	2.06	2.59	3.28	4.20	5.08	6.23
Limit (obs.)	20.8	13.6	8.81	6.63	6.41	5.21	3.94	3.29	3.25	1.82	1.55	1.96	1.89	2.11	3.17	3.27	5.77	5.53

and NSF (USA); CEA and CNRS/IN2P3 (France); FASI, Rosatom and RFBR (Russia); CNPq, FAPERJ, FAPESP and FUNDUNESP (Brazil); DAE and DST (India); Colciencias (Colombia); CONACyT (Mexico); KRF and KOSEF (Korea); CONICET and UBACyT (Argentina); FOM (The Netherlands); STFC and the Royal Society (United Kingdom); MSMT and GACR (Czech Republic); CRC Program, CFI, NSERC and WestGrid Project (Canada); BMBF and DFG (Germany); SFI (Ireland); The Swedish Research Council (Sweden); and CAS and CNSF (China).

[a] Visitor from Augustana College, Sioux Falls, SD, USA.
[b] Visitor from The University of Liverpool, Liverpool, UK.
[c] Visitor from SLAC, Menlo Park, CA, USA.
[d] Visitor from ICREA/IFAE, Barcelona, Spain.
[e] Visitor from Centro de Investigacion en Computacion - IPN, Mexico City, Mexico.
[f] Visitor from ECFM, Universidad Autonoma de Sinaloa, Culiacán, Mexico.
[g] Visitor from Universität Bern, Bern, Switzerland.

[8] R. Barate *et al.*, Phys. Lett. B **565**, 61 (2003).
[9] The LEP Electroweak Working Group, the Tevatron Electroweak Working Group, the SLD electroweak and heavy flavour groups, arXiv:0911.2604 [hep-ex].
[10] T. Han, A. Turcot, and R-J. Zhang, Phys. Rev. D **59**, 093001 (1999); M. Carena *et al.* (Higgs Working Group Collaboration), arXiv:hep-ph/0010338.
[11] V. Abazov *et al.* (D0 Collaboration), Nucl. Instrum. Methods Phys. Res. A. **565**, 463 (2006); M. Abolins *et al.*, Nucl. Instrum. Methods Phys. Res. A **584/1**, 75 (2007); R. Angstadt *et al.*, arXiv:0911.2522 [physics.ins-det] (submitted to Nucl. Instrum. Methods Phys. Res. A).
[12] T. Aaltonen *et al.* Phys. Rev. Lett. **102**, 021802 (2009).
[13] V. Abazov *et al.* (D0 Collaboration), Phys. Rev. Lett. **96**, 011801 (2006).
[14] T. Aaltonen *et al* (CDF Collaboration),arXiv:1001.4468 [hep-ex] (submitted to Phys. Rev. Lett.).
[15] V. Abazov *et al.* (D0 Collaboration), Phys. Rev. Lett. **102**, 051803 (2009); Phys. Lett. B **655**, 209 (2007).
[16] M.L. Mangano *et al.*, JHEP **0307**, 001 (2003); we use version 2.11.
[17] T. Sjöstrand *et al.*, Comput. Phys. Commun. **135**, 238 (2001); we use version 6.323 or later.
[18] J. Pumplin *et al.*, JHEP **07**, 012 (2002).
[19] R. Brun and F. Carminati, CERN Program Library Long Writeup W5013, 1993 (unpublished).
[20] R. Hamberg, W.L. van Neerven, and T. Matsuura, Nucl. Phys. **B359**, 343 (1991) [Erratum-ibid. **644**, 403 (2002)].
[21] A.D. Martin, R.G. Roberts, W.J. Stirling, and R.S. Thorne, Phys. Lett. B **604**, 61 (2004).
[22] S. Moch and P. Uwer, Phys. Rev. D **78**, 034003 (2008); we use $\sigma(t\bar{t}) = 7.88$ pb.
[23] J.M. Campbell and R.K. Ellis, Phys. Rev. D **60**, 113006 (1999); we use $\sigma(WW) = 11.66$ pb, $\sigma(WZ) = 3.45$ pb, and $\sigma(ZZ) = 1.37$ pb.
[24] C. Anastasiou, R. Boughezal, and F. Petriello, JHEP **0904**, 003 (2009); D. de Florian and M. Grazzini, Phys. Lett. B **674**, 291 (2009); K. A. Assamagan *et al.*, arXiv:hep-ph/0406152; O. Brein, A. Djouadi, and R. Harlander, Phys. Lett. B **579**, 149 (2004); M. L. Ciccolini, S. Dittmaier, and M. Krämer, Phys. Rev. D **68**, 073003 (2003); E. Berger and J. Campbell, Phys. Rev. D **70**, 073011 (2004).
[25] A. Djouadi, J. Kalinowski, and M. Spira, Comput. Phys. Commun. **108**, 56 (1998).
[26] V. Abazov *et al.* (D0 Collaboration), Phys. Rev. Lett. **100**, 102002 (2008).
[27] K. Melnikov and F. Petriello, Phys. Rev. D **74**, 114017 (2006).
[28] S. Frixione and B.R. Webber, JHEP **0206**, 029 (2002).
[29] T. Binoth, M. Ciccoli, N. Kauer, and M. Krämer, JHEP **0503**, 065 (2005); JHEP **0612**, 046 (2006).
[30] T. Gleisberg *et al.*, JHEP **0402**, 056 (2004).
[31] The D0 coordinate system is cylindrical with the z-axis in the direction of the proton beam. In this frame, the angle ϕ is the azimuthal angle, and θ is the polar angle. The pseudorapidity η is defined as $\eta = -\ln[\tan(\theta/2)]$.
[32] G. Blazey *et al.*, arXiv:hep-ex/0005012v2.
[33] J. Smith, W.L. van Neerven, and J.A.M. Vermaseren, Phys. Rev. Lett. **50**, 1738 (1983).
[34] T. Gleisberg *et al.*, Phys. Rev. D **72**, 034028 (2005).
[35] T. Junk, Nucl. Instrum. Methods Phys. Res. A. **434**, 435 (1999); A. Read, J. Phys. G **28**, 2693 (2002).
[36] W. Fisher, FERMILAB-TM-2386-E.
[37] Auxiliary material appended.

Auxiliary material

Figures 1 - 4 are the distributions of variables used to define the final selection: $\Delta\phi(\ell,\ell)$, $\not\!\!E_T$, $\not\!\!E_T^{\rm Sc}$, and $M_T^{\rm min}$. The distributions are shown at final selection having removed final selection requirement on the plotted variable. Figures 5 - 15 are the distributions of variables input into the neural network at final selection.

TABLE I: Expected and observed event yields in each channel after final selection and requiring NN output > 0.9. The systematic uncertainty after fitting is shown.

NN output > 0.9			
	$e^{\pm}\mu^{\mp}$ final selection	$e^{+}e^{-}$ final selection	$\mu^{+}\mu^{-}$ final selection
Signal ($m_H = 165$ GeV)	1.9 ± 0.2	4.0 ± 0.4	2.6 ± 0.3
Total background	3.2 ± 0.1	28.1 ± 0.5	11.6 ± 0.3
Data	3	30	11

TABLE II: The production cross sections for the SM Higgs boson assumed for estimation of signal yield and the branching fraction for $H \to W^+W^-$. The gluon fusion Higgs production cross section ($\sigma_{gg} \to H$) has been determined with a NNLO calculation while all other Higgs production cross sections ($\sigma(WH)$, $\sigma(ZH)$, and $\sigma(VBF)$) were determined with a NLO calculation.

m_H (GeV)	$\sigma(gg \to H)$ (fb)	$\sigma(WH)$ (fb)	$\sigma(ZH)$ (fb)	$\sigma(VBF)$ (fb)	$B(H \to W^+W^-)$ (%)
115	1240	178.8	107.4	79.1	7.974
120	1093	152.9	92.7	71.6	13.20
125	967	132.4	81.1	67.4	20.18
130	858	114.7	70.9	62.5	28.69
135	764	99.3	62.0	57.6	38.28
140	682	86.0	54.2	52.6	48.33
145	611	75.3	48.0	49.2	58.33
150	548	66.0	42.5	45.7	68.17
155	492	57.8	37.6	42.2	78.23
160	439	50.7	33.3	38.6	90.11
165	389	44.4	29.5	36.1	96.10
170	349	38.9	26.1	33.6	96.53
175	314	34.6	23.3	31.1	95.94
180	283	30.7	20.8	28.6	93.45
185	255	27.3	18.6	26.8	83.79
190	231	24.3	16.6	24.9	77.61
195	210	21.7	15.0	23.0	74.95
200	192	19.3	13.5	21.2	73.47

TABLE III: Systematic uncertainties in percent for the Monte Carlo samples and the multijet estimate. Uncertainties are identical across all channels except where noted. The nature of the uncertainty is indicated in the last column of the table. Uncertainties that change the differential distribution of the final discriminant are labeled with "D", while uncertainties that affect only the normalization are indicated by "N". The values for uncertainties with a differential dependence correspond to the maximum amplitude of fluctuations in the final discriminant.

	Σ Bkgd	Signal	$Z+jets/\gamma$	$W+jets/\gamma$	$t\bar{t}$	Diboson	Multijet	Nature
Lepton identification	±4	±4	±4	±4	±4	±4	-	N
Lepton momentum resolution	±2	±2	±1	±1	±1	±2	-	D
Jet energy scale	±4	±1	±8	±1	±1	±1	-	D
Jet energy resolution	±3	±1	±4	±2	±1	±1	-	D
Jet identification	±4	±1	±6	±4	±1	±1	-	D
$Z-p_T$ correction	±1	-	±3	-	-	-	-	D
$W-p_T$ correction	±1	-	-	±2	-	-	-	D
Diboson NLO correction	±1	±1	-	-	-	±1	-	D
Multijet Normalization e^+e^-	±2		-	-	-	-	±20	N
Multijet Normalization $e^\pm\mu^\mp$	±1		-	-	-	-	±10	N
Multijet Normalization $\mu^+\mu^-$	±2		-	-	-	-	±20	N
Cross section	±7	±10	±6	±6	±10	±6	-	N
PDF	$\pm$ 1	±1	-	-	-	-	-	N
Luminosity	±6.1	±6.1	-	-	-	-	-	N

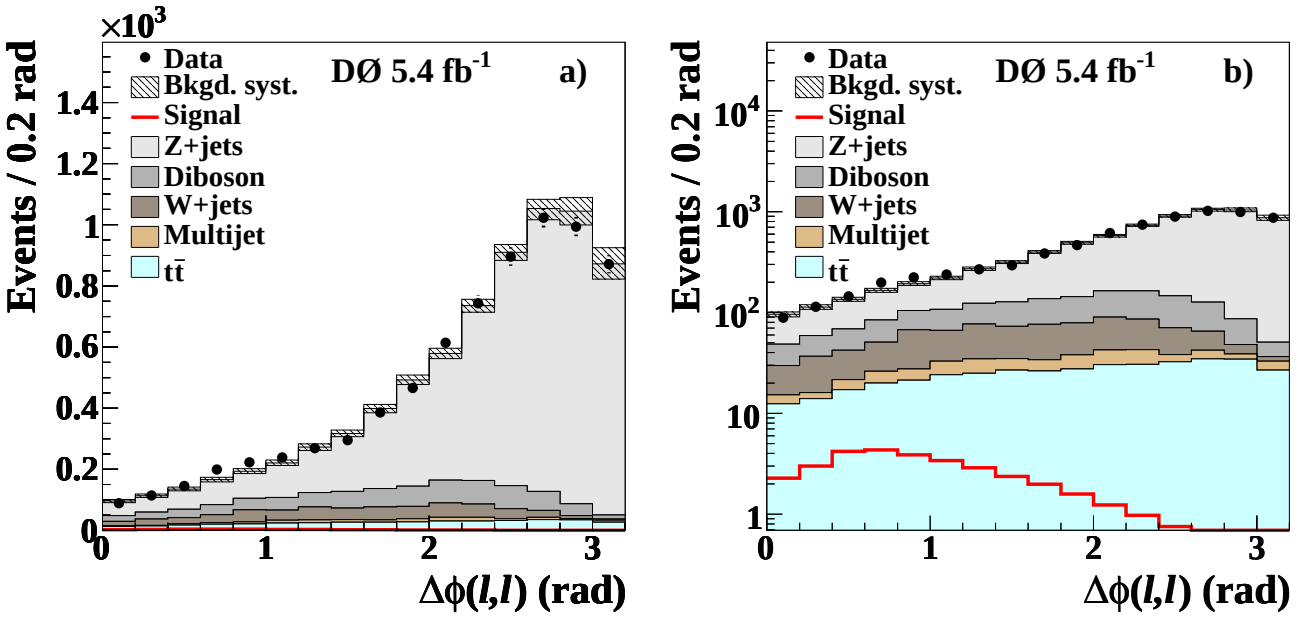

FIG. 1: The $\Delta\phi(\ell,\ell)$ angle between the two leptons after all final selection requirements except for the selection on $\Delta\phi(\ell,\ell)$ in linear (a) and logarithmic (b) scale for the combination of e^+e^-, $\mu^+\mu^-$, and $e^\pm\mu^\mp$ channels. The signal is shown for m_H=165 GeV and is scaled to the SM prediction for the combination of Higgs boson production from gluon fusion, vector boson fusion, and associated production. The systematic uncertainty is shown after fitting.

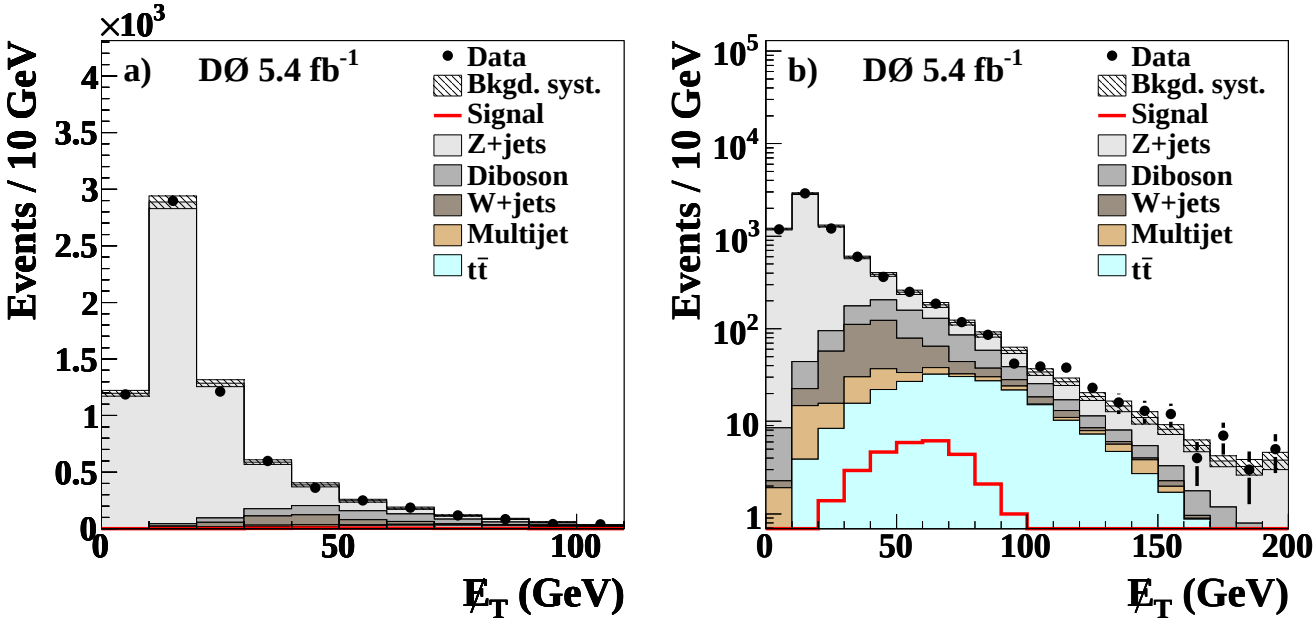

FIG. 2: The $\not\!\!E_T$ after all selections except for the selection on $\not\!\!E_T$ in linear (a) and logarithmic (b) scale for the combination of e^+e^-, $\mu^+\mu^-$, and $e^\pm\mu^\mp$ channels. The signal is shown for m_H=165 GeV and is scaled to the SM prediction for the combination of Higgs boson production from gluon fusion, vector boson fusion, and associated production. The systematic uncertainty is shown after fitting.

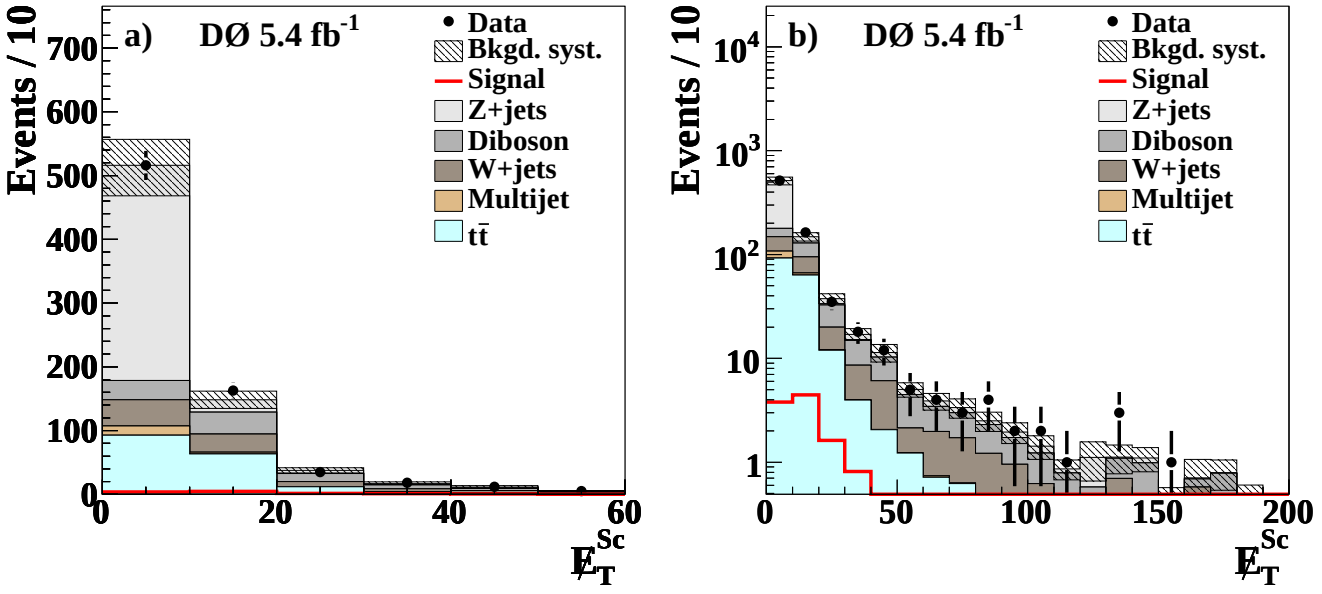

FIG. 3: The $\not\!\!E_T^{\rm Sc}$ after all selections except for the selection on $\not\!\!E_T^{\rm Sc}$ in linear (a) and logarithmic (b) scale for the combination of e^+e^-, and $e^\pm\mu^\mp$ channels. The signal is shown for m_H=165 GeV and is scaled to the SM prediction for the combination of Higgs boson production from gluon fusion, vector boson fusion, and associated production. The systematic uncertainty is shown after fitting.

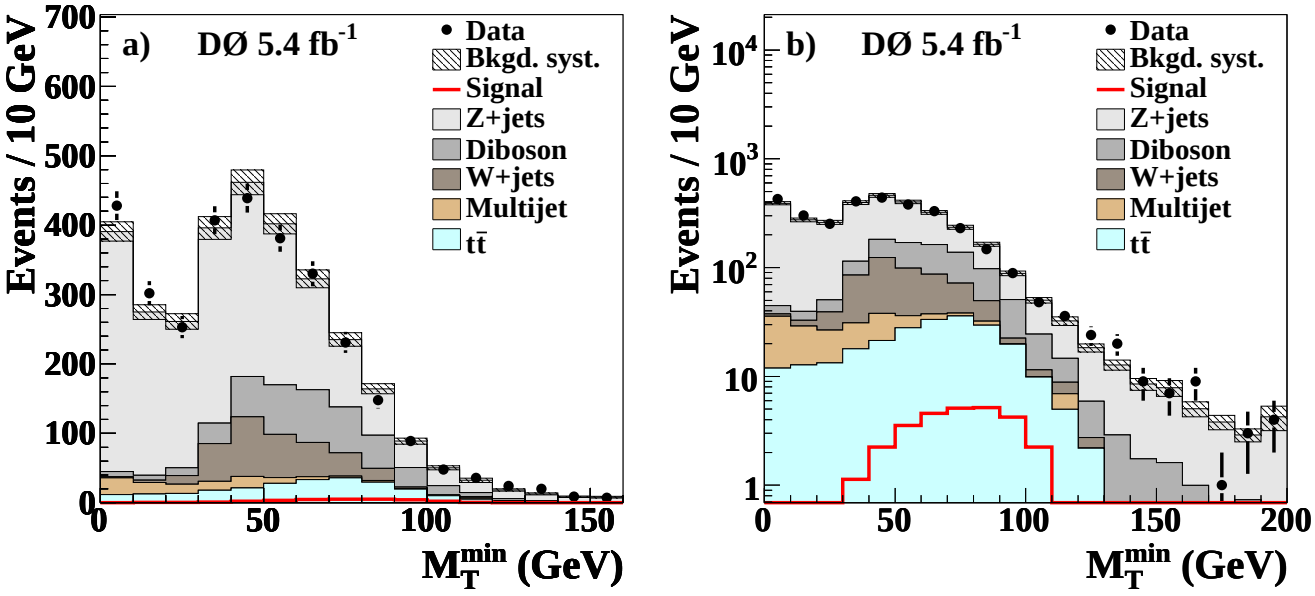

FIG. 4: The $M_T^{\rm min}$after all selections except for the selection on $M_T^{\rm min}$ in linear (a) and logarithmic (b) scale for the combination of e^+e^-, $\mu^+\mu^-$, and $e^\pm\mu^\mp$ channels. The signal is shown for m_H=165 GeV and is scaled to the SM prediction for the combination of Higgs boson production from gluon fusion, vector boson fusion, and associated production. The systematic uncertainty is shown after fitting.

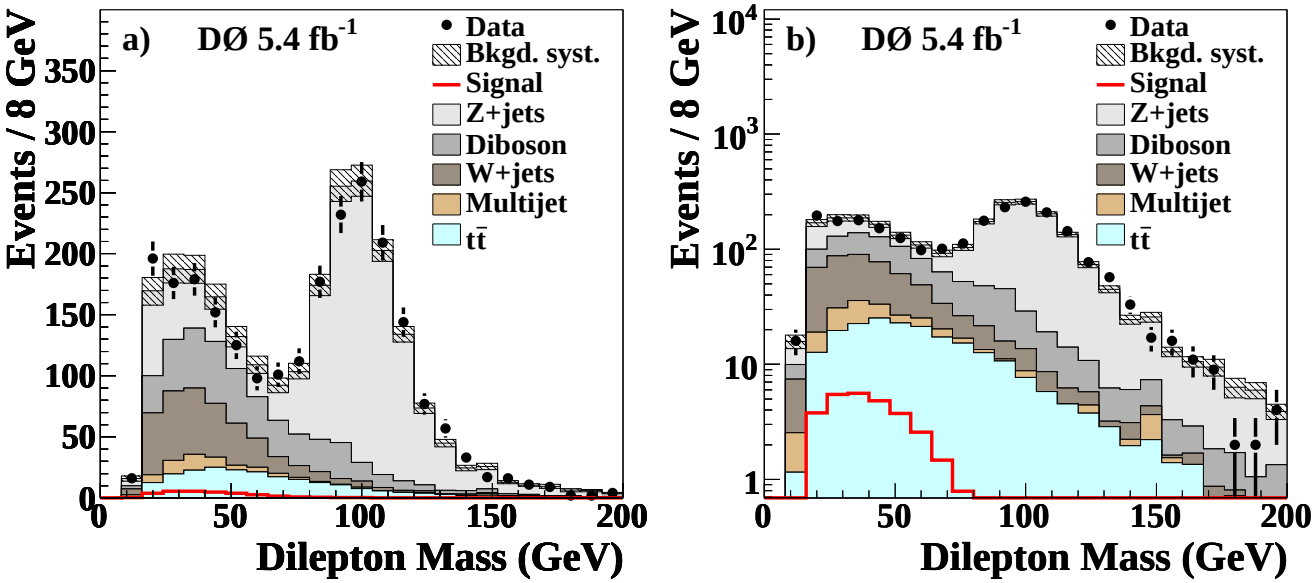

FIG. 5: The dilepton invariant mass at final selection in linear (a) and logarithmic (b) scale for the combination of e^+e^-, $\mu^+\mu^-$, and $e^\pm\mu^\mp$ channels. The signal is shown for m_H=165 GeV and is scaled to the SM prediction for the combination of Higgs boson production from gluon fusion, vector boson fusion, and associated production. The systematic uncertainty is shown after fitting.

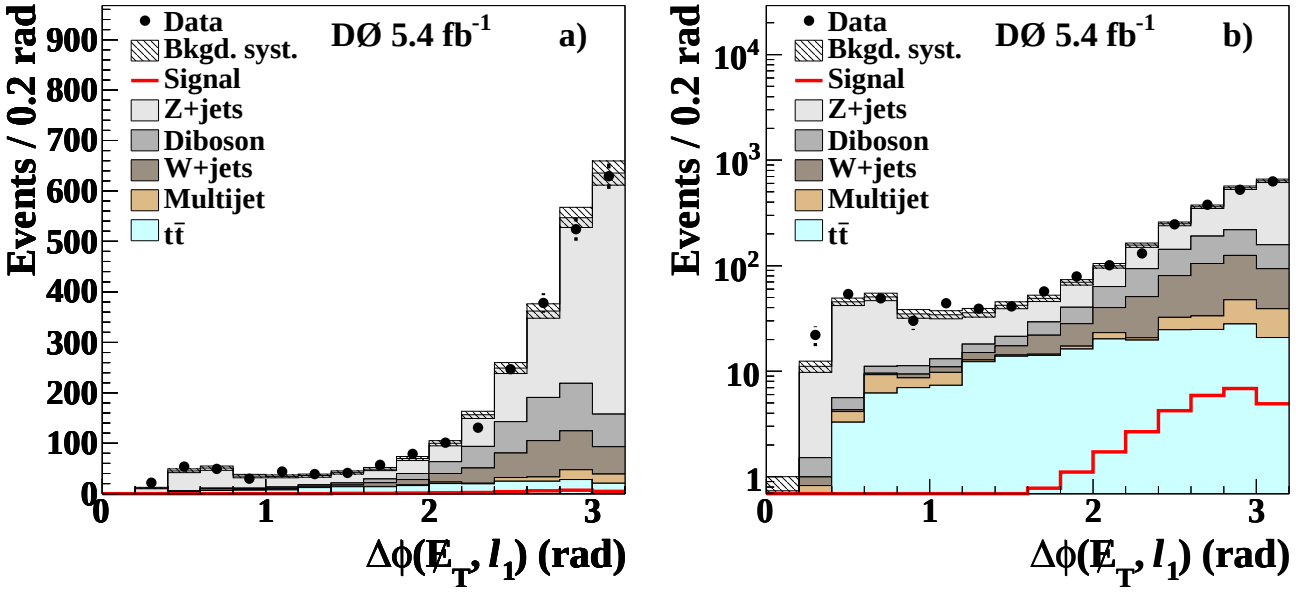

FIG. 6: The $\Delta\phi(\not\!\!E_T, \ell_1)$ at final selection in linear (a) and logarithmic (b) scale for the combination of e^+e^-, $\mu^+\mu^-$, and $e^\pm\mu^\mp$ channels. The signal is shown for m_H=165 GeV and is scaled to the SM prediction for the combination of Higgs boson production from gluon fusion, vector boson fusion, and associated production. The systematic uncertainty is shown after fitting.

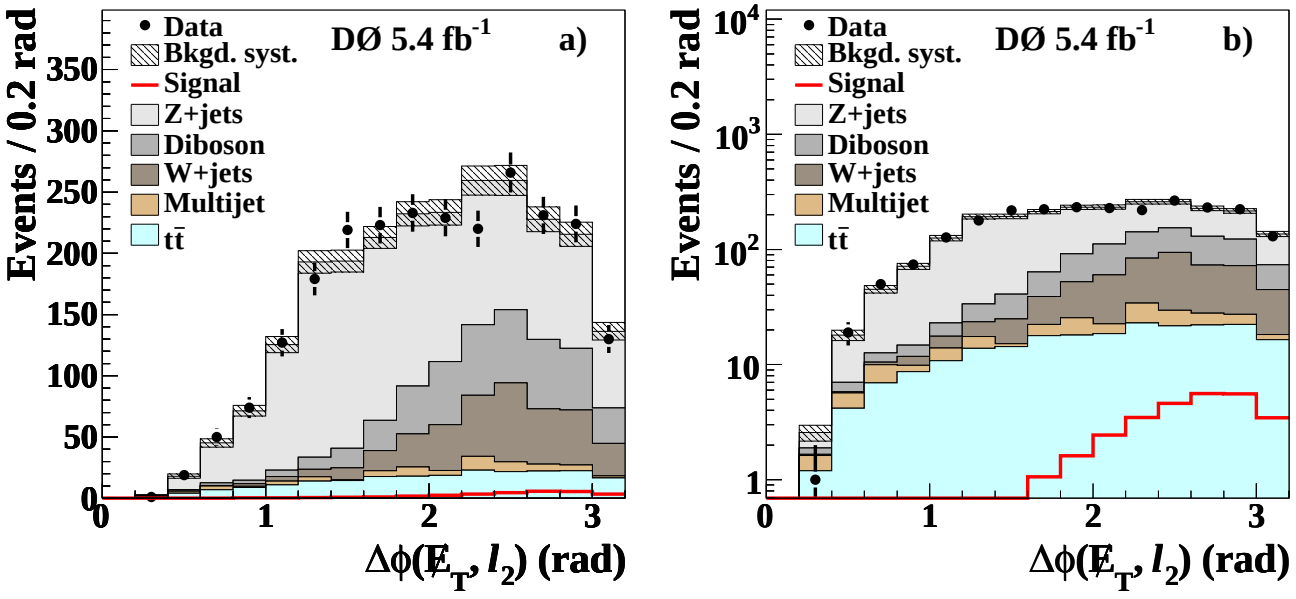

FIG. 7: The $\Delta\phi(\not\!\!E_T, \ell_2)$ at final selection in linear (a) and logarithmic (b) scale for the combination of e^+e^-, $\mu^+\mu^-$, and $e^\pm\mu^\mp$ channels. The signal is shown for m_H=165 GeV and is scaled to the SM prediction for the combination of Higgs boson production from gluon fusion, vector boson fusion, and associated production. The systematic uncertainty is shown after fitting.

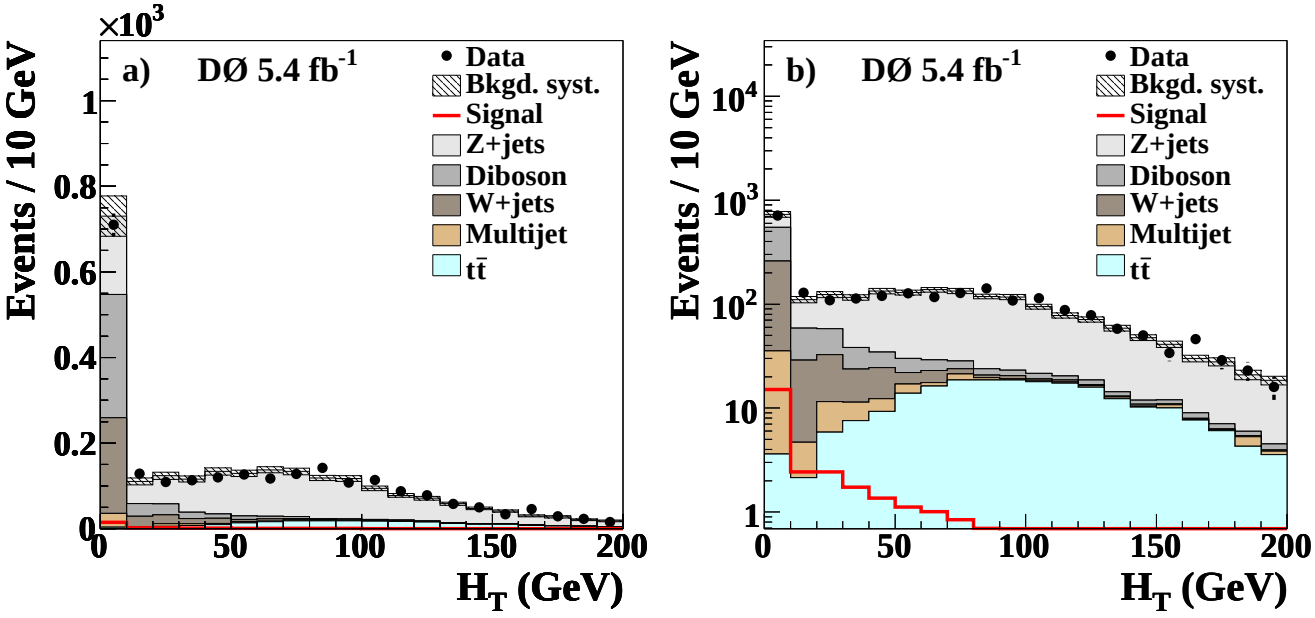

FIG. 8: The scalar sum of the transverse momenta of the jets at final selection in linear (a) and logarithmic (b) scale for the combination of e^+e^-, $\mu^+\mu^-$, and $e^\pm\mu^\mp$ channels. The signal is shown for m_H=165 GeV and is scaled to the SM prediction for the combination of Higgs boson production from gluon fusion, vector boson fusion, and associated production. The systematic uncertainty is shown after fitting.

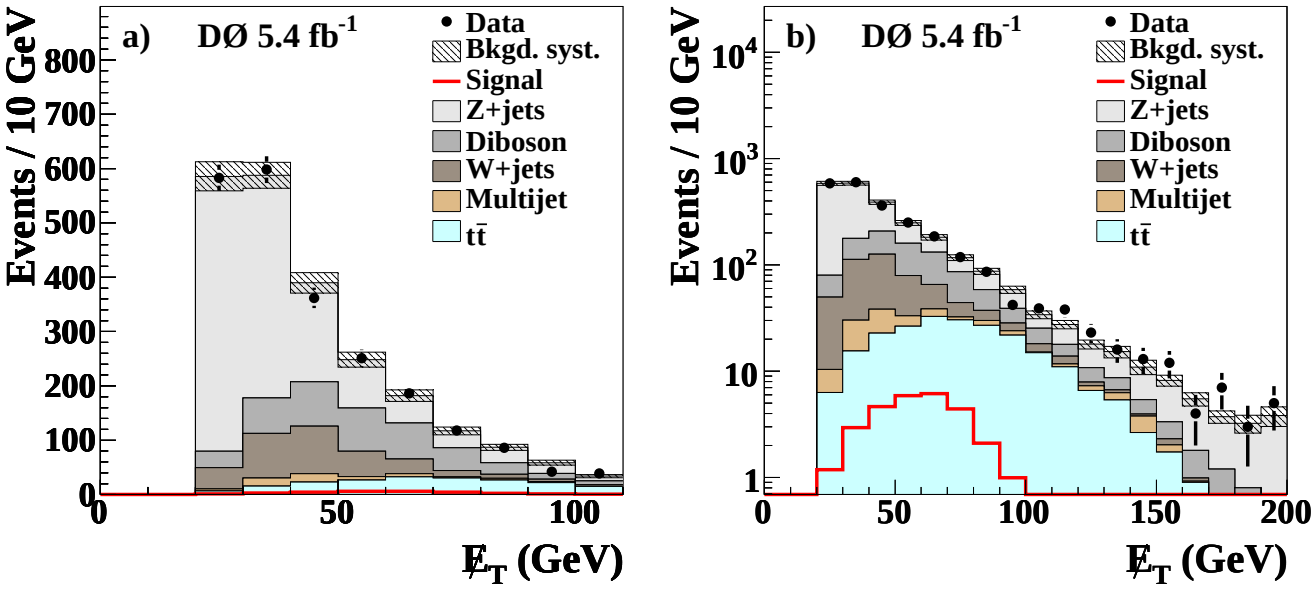

FIG. 9: The $\not\!\!E_T$ at final selection in linear (a) and logarithmic (b) scale for the combination of e^+e^-, $\mu^+\mu^-$, and $e^\pm\mu^\mp$ channels. The signal is shown for m_H=165 GeV and is scaled to the SM prediction for the combination of Higgs boson production from gluon fusion, vector boson fusion, and associated production. The systematic uncertainty is shown after fitting.

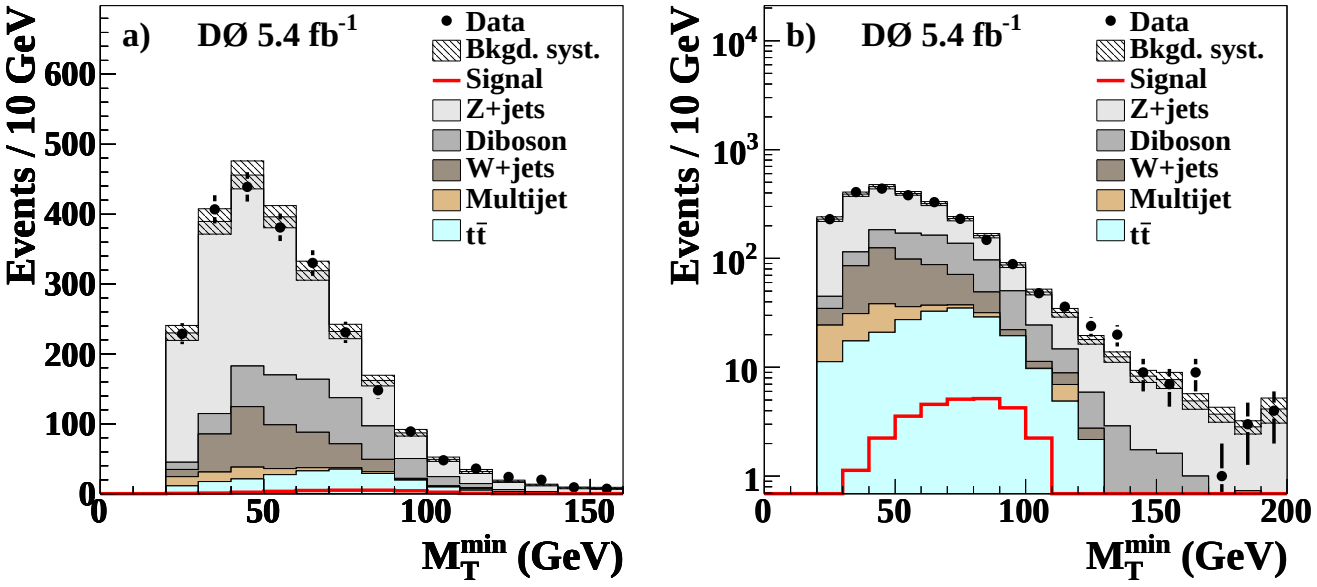

FIG. 10: The $M_T^{\rm min}$ at final selection in linear (a) and logarithmic (b) scale for the combination of e^+e^-, $\mu^+\mu^-$, and $e^\pm\mu^\mp$ channels. The signal is shown for m_H=165 GeV and is scaled to the SM prediction for the combination of Higgs boson production from gluon fusion, vector boson fusion, and associated production. The systematic uncertainty is shown after fitting.

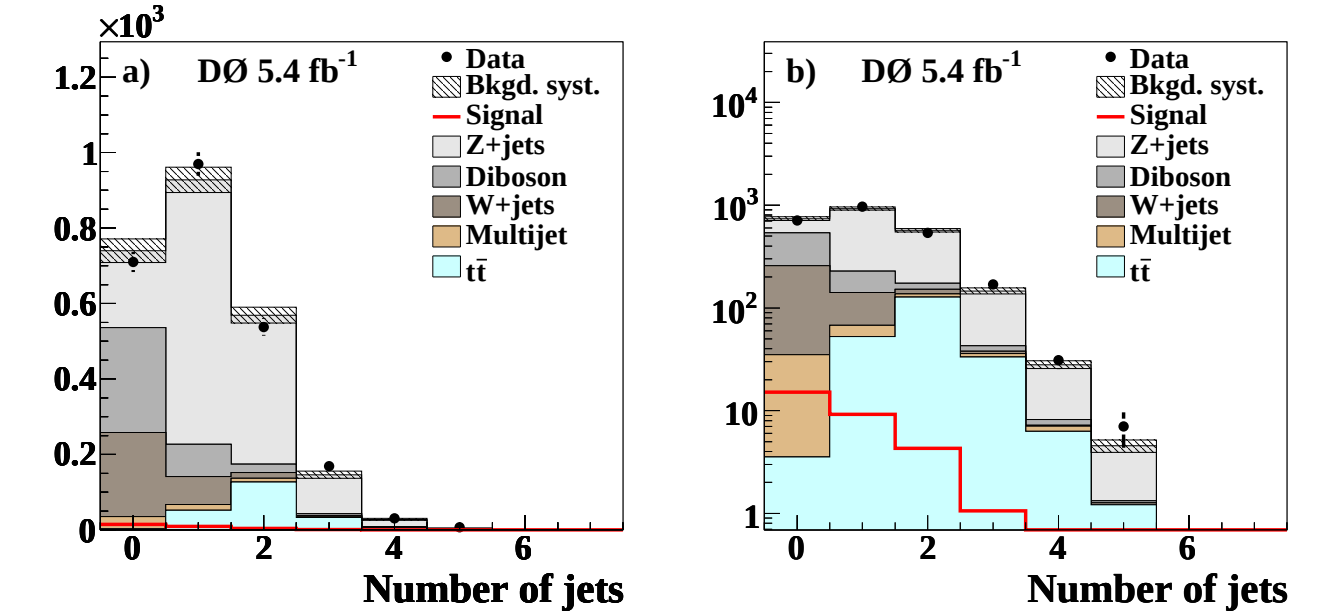

FIG. 11: The number of identified jets at final selection in linear (a) and logarithmic (b) scale for the combination of e^+e^-, $\mu^+\mu^-$, and $e^\pm\mu^\mp$ channels. The signal is shown for m_H=165 GeV and is scaled to the SM prediction for the combination of Higgs boson production from gluon fusion, vector boson fusion, and associated production. The systematic uncertainty is shown after fitting.

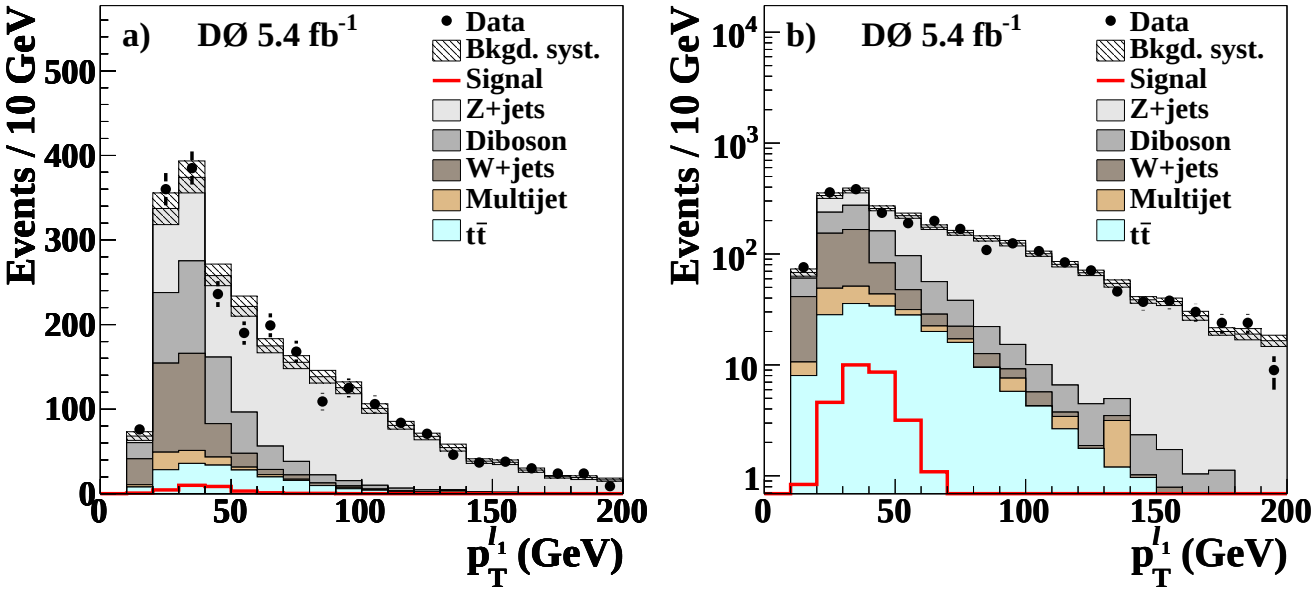

FIG. 12: The transverse momentum of the leading lepton at final selection in linear (a) and logarithmic (b) scale for the combination of e^+e^-, $\mu^+\mu^-$, and $e^\pm\mu^\mp$ channels. The signal is shown for m_H=165 GeV and is scaled to the SM prediction for the combination of Higgs boson production from gluon fusion, vector boson fusion, and associated production. The systematic uncertainty is shown after fitting.

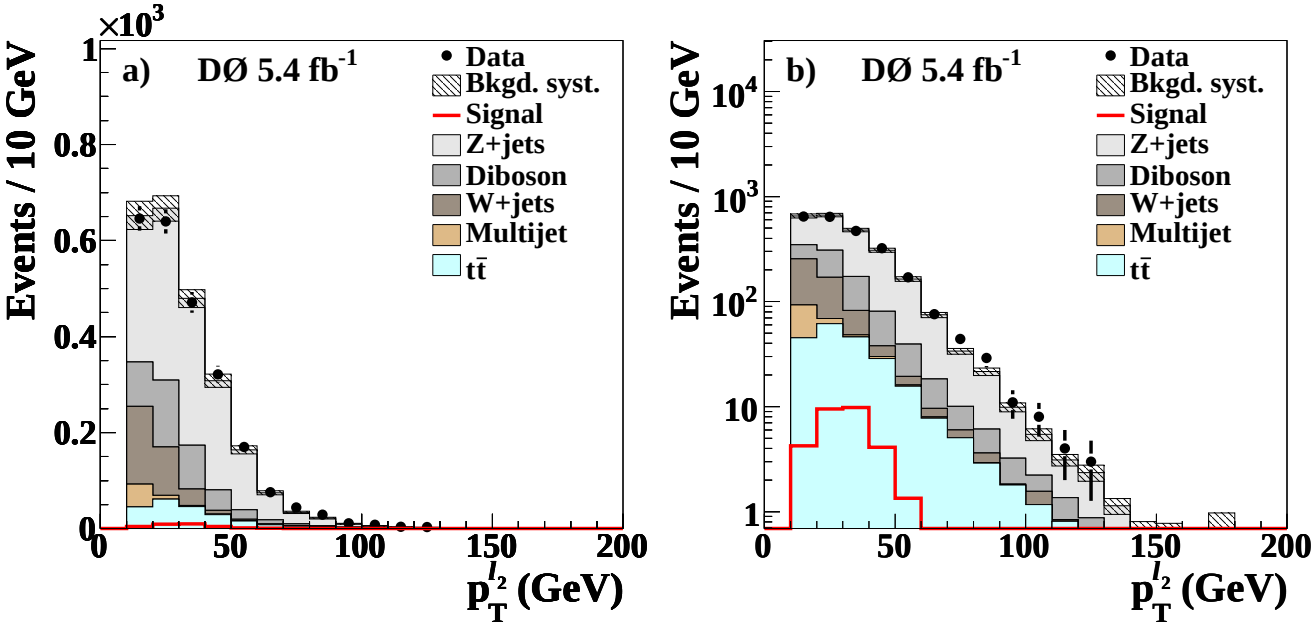

FIG. 13: The transverse momentum of the next-to-leading lepton at final selection in linear (a) and logarithmic (b) scale for the combination of e^+e^-, $\mu^+\mu^-$, and $e^\pm\mu^\mp$ channels. The signal is shown for m_H=165 GeV and is scaled to the SM prediction for the combination of Higgs boson production from gluon fusion, vector boson fusion, and associated production. The systematic uncertainty is shown after fitting.

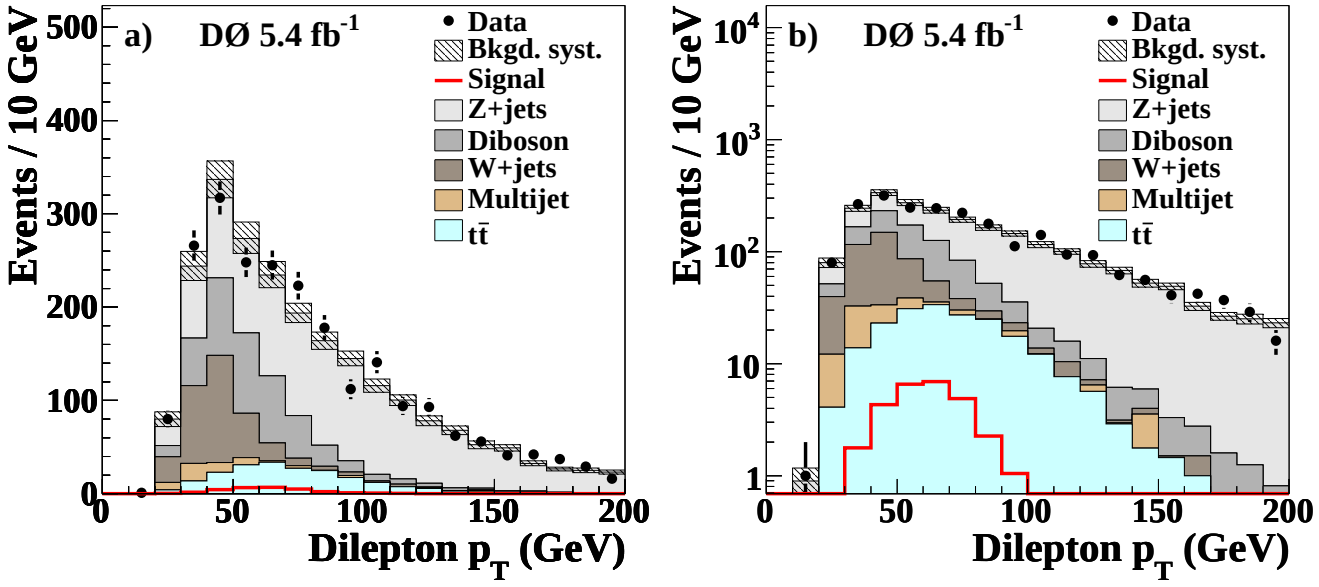

FIG. 14: The transverse momentum of the dilepton system at final selection in linear (a) and logarithmic (b) scale for the combination of e^+e^-, $\mu^+\mu^-$, and $e^\pm\mu^\mp$ channels. The signal is shown for m_H=165 GeV and is scaled to the SM prediction for the combination of Higgs boson production from gluon fusion, vector boson fusion, and associated production. The systematic uncertainty is shown after fitting.

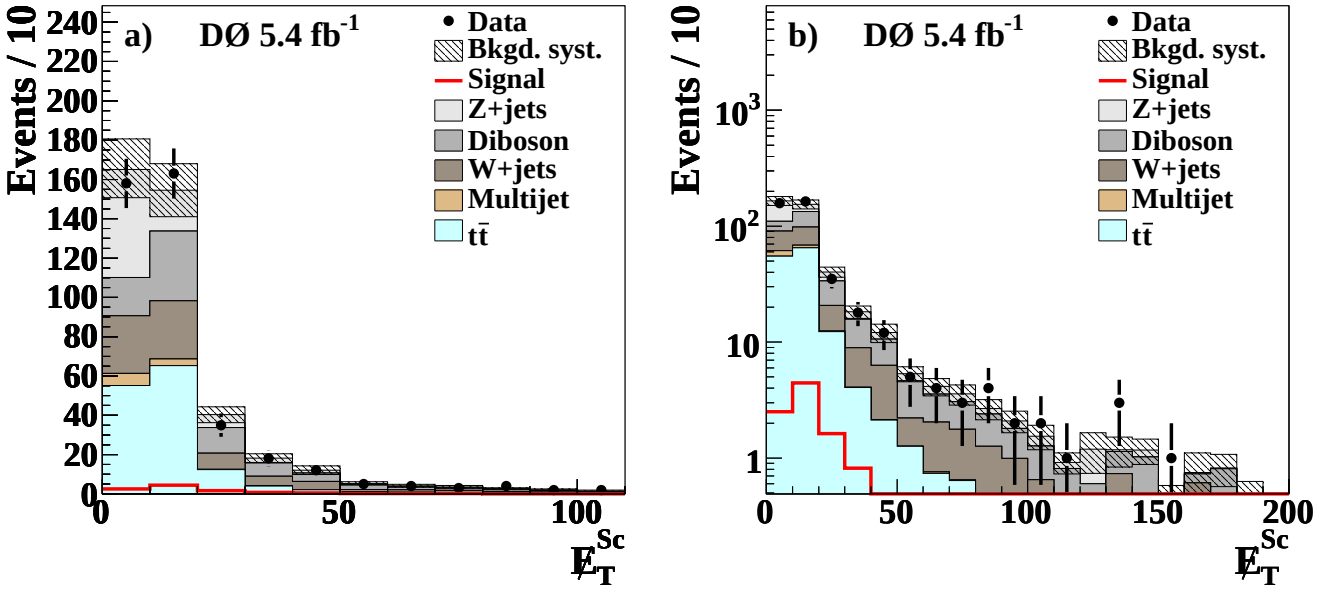

FIG. 15: The $\not\!\!E_T^{\rm Sc}$ at final selection in linear (a) and logarithmic (b) scale for the combination of e^+e^- and $e^\pm\mu^\mp$ channels. The signal is shown for m_H=165 GeV and is scaled to the SM prediction for the combination of Higgs boson production from gluon fusion, vector boson fusion, and associated production. The systematic uncertainty is shown after fitting.